Proceedings of the 12th International Conference on
Aluminium Alloys, September 5-9, 2010, Yokohama, Japan
©2010 The Japan Institute of Light Metals
pp. 2335-2340

Coupled Surface and Microstructural Observations of Damage Accumulation during Bending of Al-Mg-Si Alloys

Alastair Wise[1], Toni Chezan[1], Jan Pool[1], Radhakanta Rana[1] and Peter De Smet[2]
[1]Corus RD&T, PO Box 10000, 1970CA IJmuiden, Netherlands
[2]Aleris Aluminum Duffel BVBA, A. Stocletlaan 87, 2570 Duffel, Belgium

The bendability of 6xxx series Al-Mg-Si alloys can become more challenging as the strength of the alloy increases, therefore understanding the mechanism of damage accumulation and eventual failure is an important first step in improving the bendability of a given alloy. In this paper a series of experiments on AA6016 T4P sheet samples are described that couple optical and SEM observations of the outer surface of a bend sample and the concomitant microstructural development during bending to failure. These observations demonstrate that the failure mechanism of the alloy, and thus the bendability, is strongly influenced not only by chemistry but also by processing. Of particular relevance are the grain boundary regions where it was clearly seen that strain localization during bending promoted failure on the grain boundary, leading to poorer bending performance. The differences in damage evolution between samples displaying good and bad bending performance are discussed and mechanisms to explain these differences are proposed.

Keywords: *automotive sheet, bending, microstructure*

1. Introduction

In the current drive to reduce CO_2 emissions, OEMs and their Tier 1 suppliers are actively looking for new and improved materials that can offer a reduction in vehicle mass. Research shows [1] that a 100 kg reduction in vehicle mass gives a direct reduction of around nine grams of CO_2 per kilometre. Based on a typical usage of 12,000 km per year, this would result in a reduction of 108 kg of CO_2 emissions for every year the vehicle is in use. For this reason, aluminium alloys, in particular those based on the Al-Mg-Mn (5xxx) and Al-Mg-Si (6xxx) series, have found widespread use in the automotive industry and this utilisation is predicted to increase into the next decade [2]. At present, closure applications tend to dominate 6xxx usage, where the favourable combination of formability, bendability, surface quality and strength after paint-bake make them an attractive choice.

Hoods are a key market for the heat-treatable 6xxx alloys and here there is an increasing demand for higher strength alloys to permit down-gauging and therefore additional weight saving [3]. Within the well known AA6016 composition range, this increase in strength must be carefully balanced with the formability and bendability to ensure that the correct balance remains; in particular the bendability in the T4P temper is of paramount importance as the hood outer and inner panels are connected to each other with a hemming operation [4]. During this hemming operation the outer fibres of the sheet are subjected to extremely localised straining and as a general rule, the higher the alloy strength, the more susceptible it is to failure during hemming. An important first step in improving the hemmability of a given alloy is to understand how it fails and the key microstructural features that control the failure. This paper describes an experimental procedure used to observe the failure during hemming of several AA6016 T4P alloy variants and attempts to propose explanations for the differences observed.

2. Experimental Procedure

2.1 Alloy Chemistry and Processing

Sheets of 1mm thick AA6016A T4P were produced from a single industrial direct chill cast slab, with the thermo-mechanical processing varied according to two parallel laboratory production routes. The processing conditions used were selected to produce samples with both good and bad hemmability, according to proprietary production practices used by Aleris Aluminum Duffel. The two processing routes used were arbitrarily named Route A (good hemming) and Route B (bad hemming). The chemical composition is given in Table 1.

Table 1: Sheet Composition (wt%)

Si	Fe	Cu	Mn	Mg	Cr	Ti
0.9	0.2	0.18	0.18	0.6	≤0.05	≤0.05

The composition was selected to give a 0.2% proof strength of at least 250 MPa after paint-bake. A deleterious concomitant effect of this high strength can be a reduced hemmability in the T4P condition [5] and an increased tendency for natural ageing [6], which also can contribute to a reduction in hemmability. Both processing routes used the same pre-ageing cycle and samples for both routes were tested approximately 12 months after solution heat-treatment and pre-ageing, thereby eliminating natural ageing as an additional variable between the two sets of samples. For both routes, the 0.2% proof stress was measured at around 160 MPa and the ultimate tensile strength was 280 MPa i.e. there was no appreciable difference in tensile properties between the two variants.

2.2 Sample Hemming and Surface - Microstructural Coupled Observations

Samples of material from each process route were hemmed to angles of 135°, 150° and 180°, using a former with a 0.2mm radius, with samples oriented in RD and TD directions (note that the RD samples have the bend axis perpendicular to the rolling direction and vice versa for the TD samples). The aim of hemming to three different angles was to effectively capture the initiation and growth of cracks as the hemming operation progressed. The samples were also visually examined to determine the extent of surface roughening. Figure 1 presents the outer surfaces of the samples.

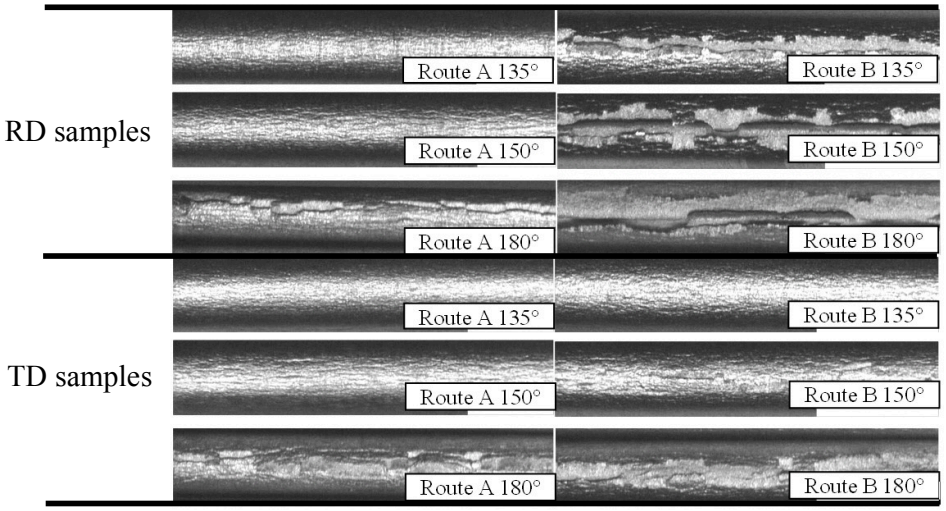

Fig. 1: Outer Surface of Hemmed Samples (top row RD orientation, bottom row TD orientation)

Examination of the samples presented in Figure 1 shows quite clearly that samples processed according to Route A show significantly better hemming behaviour than those processed following Route B, in particular the RD samples: at a bend angle of 150° the Route A samples show surface roughening only whereas the Route B samples have already begun to crack.

Samples from Route A and Route B material were then prepared for metallographic examination to characterise the microstructural differences between the two processing routes. Samples were initially taken from unstrained regions to determine the microstructural conditions before hemming. Of particular interest were the grain boundary regions and the Fe-rich particle distributions as several authors, for example [7], have identified these as being strongly linked to hemming performance. Table 2 presents the results of particle analysis of the two processing routes.

Table 2: Particle Analysis Fe-rich Intermetallics

Sample and Orientation		Average size (µm²)	Area (%)	Number Density (1/mm²)
Route A	RD-ND	2.8	0.58	2067
	TD-ND	2.7	0.54	1961
Route B	RD-ND	1.1	0.35	3084
	TD-ND	1.4	0.40	2759

The data presented in Table 2 show that there is a difference between the two materials, with Route A material having larger but more widely spaced Fe-rich particles, whereas Route B processing gives small intermetallics but a higher number density. Figure 2 shows the typical distribution of Fe-rich phases for Route A and Route B samples.

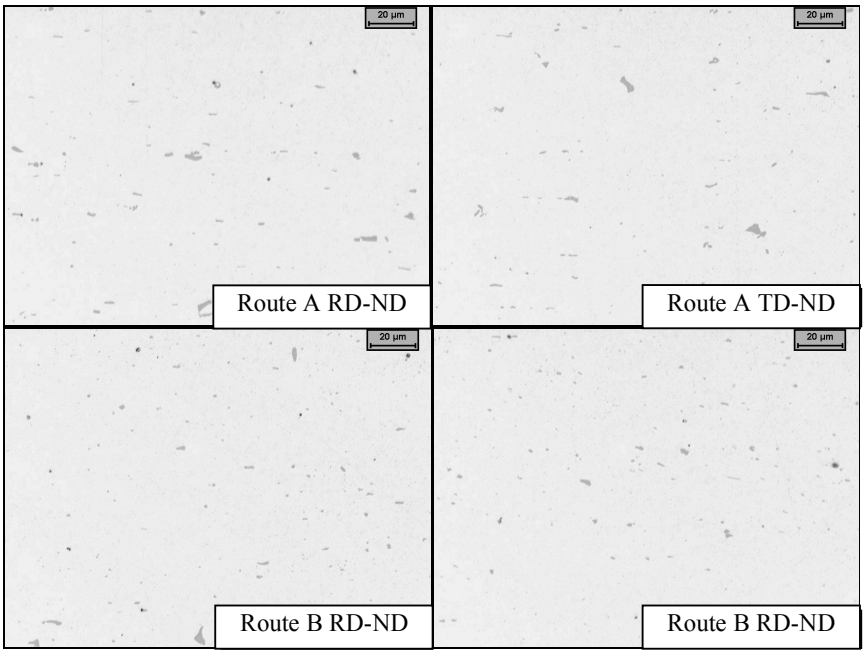

Fig. 2: Distribution of Fe-rich Particles

Etching the samples presented in Figure 2 with HF showed further differences between Route A and Route B, in particular the grain boundaries of Route B material were attacked much more readily

by the etchant, suggesting compositional differences between the grain boundary and matrix regions. These micrographs are presented in Figure 3.

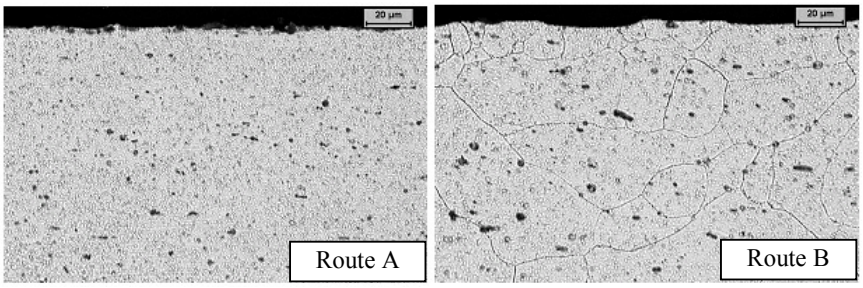

Fig. 3: Etched Grain Structures

Additional bend samples were then prepared with the outer surfaces polished prior to hemming. This polishing was performed to facilitate SEM examination of the outer surfaces at the predetermined angles during the hemming operation. As well as these surface observations, metallographic cross sections were made at the point(s) of crack initiation and growth and SEM fractography was also performed to characterise the crack growth mode. Examination of Route A material was performed first and crack initiation and growth was observed to be typically transgranular, with micro dimpling visible on the fracture surfaces. The polished outer surface of this material showed significant amounts of strain accumulation within the grains, as evidenced by the heavily deformed grains, with fine shear banding appearing to be the predominant deformation mode. Sample cracking and eventual failure initiated at one or more of the observed shear bands. In contrast, Route B material showed a strong tendency for intergranular cracking, which was confirmed through fractography on the failed samples. SEM observations on the surface of Route B material during hemming also showed that although shear banding was present, it was much less developed and the slip produced through shearing was not accumulated in the grain interior, but became localised on the grain boundaries, leading to failure of the grain boundary regions and consequently intergranular material failure. Figure 4 presents an overview of the optical and SEM images.

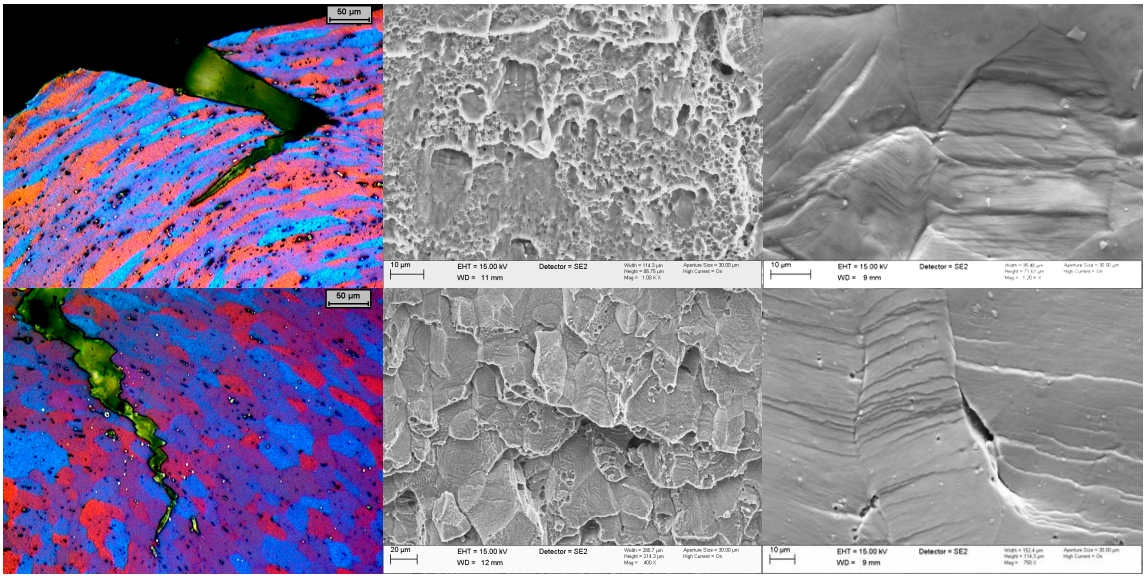

Fig. 4: Optical and SEM Images. Top row Route A, bottom row Route B. Left column Barker's etch, middle column fracture surfaces, right column outer surfaces. Both samples bent to 180°.

3. Discussion

The observations made during the course of this evaluation have shown that through careful selection of alloy processing, samples of an identical alloy can be produced with markedly different hemming performance. It is clear that the failure mechanism during hemming differs for the two materials, giving rise to transgranular failure for Route A and intergranular failure for Route B. For improved hemming performance, it is clear that a transgranular failure mode is preferred.

Based on these observations, it is apparent that significant differences in slip behaviour exist between the two materials, and this difference appears to be the determining factor in whether the sample fails in an intergranular or transgranular manner. Slip is influenced most strongly by the cluster or precipitate structure [8] therefore samples from Route A and Route B material was prepared for TEM examination to characterise the matrix and grain boundary precipitate state. The samples prepared were examined using a high angle annular dark field (HAADF) imaging technique.

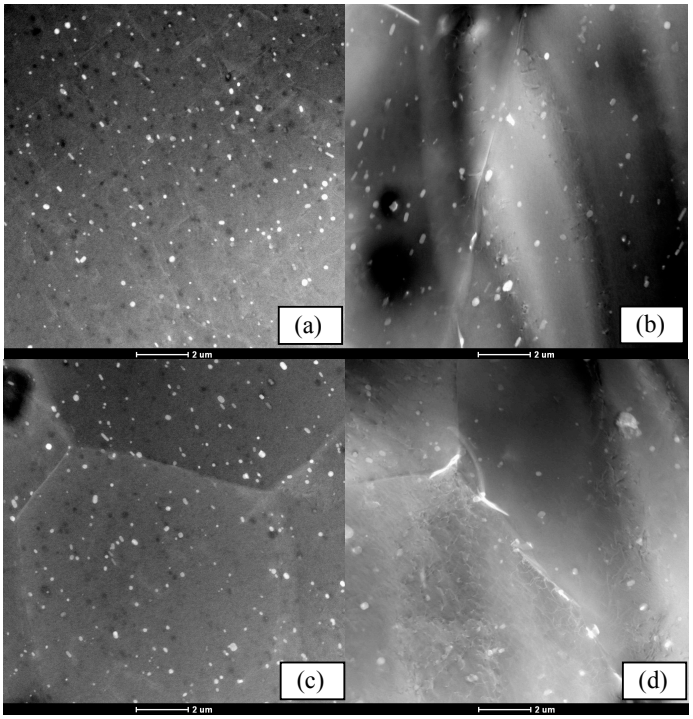

Fig. 5: HDAAF TEM images. (a) Route A matrix, (b) Route B matrix, (c) Route A grain boundary, (d) Route B grain boundary. Scale bar is 2μm.

The HDAAF TEM images, presented in Figure 5, clearly show that Route A material has a higher number density of small precipitates in the matrix compared to Route B. Based on the size of these precipitates, it is considered that these are too large to be shearable as they appear larger than 2.5nm, which has been established as a threshold for shearing [8]. Also of importance is the presence of large precipitates on the grain boundaries of the Route B material. EDX analysis of these precipitates indicated that they are most likely AlMgSiCu Q-phase. In contrast the grain boundaries of Route A material are clean with no evidence of grain boundary precipitation. The improved hemming of sample processed through Route A can therefore be attributed to a combination of the high number density of non-shearable precipitates and clean grain boundaries. The presence of non-shearable precipitates enables a more homogenous slip process [8] enabling the matrix to undergo more severe deformation prior to failure. The lack of these precipitates in Route B material will expose the grain

boundaries to greater strain localization and this combined with the grain boundary precipitation will significantly reduce the energy required to induce failure at the grain boundaries. It should be pointed out that whilst slip bands are also present in Route B material, but they appear less developed, presumably because failure at the grain boundary effectively unloads the matrix and localises strain at the boundary. It is a matter of speculation as to whether Route B material would improve if either the matrix precipitation was more similar to Route A, or if the grain boundaries were cleaner (in other words, which feature has the strongest effect on hemming performance?). Texture analysis would also be useful in determining the relative ease of deformation of a given grain in relation to its nearest neighbours.

The Fe-rich intermetallic particles did not appear to play a significant role in crack initiation and failure. Fracture and voiding of the intermetallic particles was observed but did not appear to participate in the crack initiation and propagation process. This suggests that a reduction in the iron content would not be expected to improve the hemming performance.

4. Conclusions

Samples of AA6016A T4P sheet have been produced using two differing thermo-mechanical processing routes and the hemmability of these samples was evaluated. Through a combination of metallographic examination and SEM fractography and surface observations the failure mechanisms associated with good and bad hemmability were identified, along with the key microstructural features that control hemmability. A high number density of non-shearable precipitates in the matrix is preferred to prevent strain localisation and allow the matrix to undergo greater deformation and clean boundaries increase the energy required to initiate grain boundary failure, promoting instead a more favourable transgranular failure mode.

References

[1] European Aluminium Association, *Aluminium in Cars*, (European Aluminium Association, 2007) pp. 2.
[2] SAE International, *Automotive Engineering International*, (SAE International, 2009) pp. 16-22.
[3] W. S. Miller, L. Zhuang, J. Bottema, A. J. Wittebrood, P. De Smet, A. Haszler, K. Vieregge, Materials Science and Engineering A 280 (2000) 37-49.
[4] L. Mattei, D. Daniel, G. Guiglionda and H. Klöcker, *Proceedings International Conference on Aluminium Alloys 11*, (Wiley-VCH, Weinhem, 2008) pp. 1829-1835.
[5] D. J. Lloyd, *Proceedings Automotive Alloys 1999*, (TMS, 2000) pp. 211-221.
[6] S. Esmaeili, D. J. Lloyd, W. J. Poole, Acta Materialia 51 (2003) 3467-3481.
[7] W. K. Lievers, A. K. Pilkey, D. J. Lloyd, Materials Science and Engineering A361 (2003) 312-320.
[8] W.J. Poole, X. Wang, D.J. Lloyd, J.D. Embury, Phil. Mag. 85 (2005) 3113-3135.